Materials Chemistry and Physics 254 (2020) 123377

Contents lists available at ScienceDirect

Materials Chemistry and Physics

journal homepage: www.elsevier.com/locate/matchemphys

Corrosion behavior of novel Titanium-based high entropy alloys designed for medical implants

S. Gurel [a], M.B. Yagci [b], B. Bal [c], D. Canadinc [a,*]

[a] Koc University, Advanced Materials Group (AMG), Department of Mechanical Engineering, Istanbul, 34450, Turkey
[b] Koc University Surface Science and Technology Center (KUYTAM), Istanbul, 34450, Turkey
[c] Abdullah Gül University, Department of Mechanical Engineering, Kayseri, 38080, Turkey

HIGHLIGHTS

- Static biocompatibility of TiTaHf-based high entropy alloys was investigated.
- Zr and Nb in the TiTaHf-based samples enhanced corrosion performance.
- Biomedical potential of TiTaHfNb, TiTaHfNbZr and TiTaHfMoZr was demonstrated.

ARTICLE INFO

Keywords:
High entropy alloy
Corrosion
Medical implant
TiTaHfNbZr
TiTaHfMoZr
TiTaHfNb

ABSTRACT

This paper reports on the corrosion behavior of three TiTaHf-based high entropy alloys (HEAs) in simulated body fluid (SBF) and artificial saliva (AS) in order to assess their potential utility as implant materials. Specifically, TiTaHfNb, TiTaHfNbZr and TiTaHfMoZr HEAs were subjected to static immersion experiments in SBF and AS, and both the surfaces of the samples and the immersion fluids were thoroughly examined with the state of the art techniques. The experimental results presented herein revealed that the presence of Zr and Nb in the TiTaHf-based samples enhanced corrosion performance with reduced ion release and better surface properties, while Mo addition resulted in an inhomogeneous microstructure, leading to dendrite structures and significant amount of ion release upon immersion in both media. Furthermore, a protective passive layer formation or crystallization was present on all HEA surfaces, implying that corrosion resistance can be sustained in long-term applications. Overall, the set of findings presented herein constitute an early indication of the potential of the TiTaHf-based HEAs to be utilized as implant materials.

1. Introduction

Discovery of the least chemically active, non-irritating and non-toxic materials that can interact with target tissue have made a significant contribution to the development of biomaterials [1,2]. Among metallic, ceramic and polymeric biomaterials [3,4], metallic alloys emerge as more suitable candidates for applications aimed at repairing and supporting damaged bone tissue [5,6]. Therefore, metals are commonly preferred in orthopedic implants and orthodontic practices to support failed tissue as temporary and permanent implants [7,8]. Specifically, stainless steels, CoCr alloys, and Ti-based alloys constitute the primary choices of metallic biomaterials owing to their enhanced mechanical properties, which are beneficial for implantation applications of hard tissue such as knee joint, hip joint and dental implants [6,9,10]. Nevertheless, problems, such as toxic ion release, wear, or elastic modulus mismatch between an implant and human tissue can bring about important setbacks, especially in long-term applications [5,11,12]. For instance, two commonly utilized metallic implant materials, stainless steel and NiTi shape memory alloy, exhibit a substantial amount of Ni ion release into the bloodstream or the tissue they are in contact with, leading to adverse side effects [7,10,13,14]. Another popular metallic biomaterial, namely the Ti–6Al–4V alloy, poses a health risk in long-term usage owing to V and Al ion release with potential to harm the nervous system, in addition to possible tissue loss, implant loosening, and failure of prostheses facilitated by stress shielding effect due to modulus mismatch [15–19]. Consequently, these problems compel researchers to seek alternative metallic biomaterials with excellent corrosion resistance in aggressive environments [20,21].

* Corresponding author.
E-mail address: dcanadinc@ku.edu.tr (D. Canadinc).

https://doi.org/10.1016/j.matchemphys.2020.123377
Received 20 November 2019; Received in revised form 10 March 2020; Accepted 6 June 2020
Available online 25 June 2020

Recently, a class of alloys with high corrosion resistance, namely the high entropy alloys (HEAs), have attracted significant attention owing to their superior mechanical properties [22–26], which is a result of their relatively higher configurational entropy and ability to form a single solid phase [20,27,28]. HEAs have quickly become strong candidates for various engineering applications owing to their high strength and hardness [29–33], high thermal stability [34–36], and high fracture toughness [37,38], in addition to their excellent corrosion resistance [20,35,39]. This unique combination of superior mechanical properties are present even at cryogenic temperatures since the high configurational entropy stabilizes disarranged solid phases into a single phase [27, 32,40,41]. Recent studies mainly concentrated on understanding the mechanical behavior of HEAs, as well as their microstructural properties [30,42–45].

In general, utility of metals in biomedical applications has primarily negative effects on biocompatibility owing to their corrosion tendency, which can damage both the implant, and the surrounding tissue and organs [46]. Besides, the pH of the surrounding environment can vary easily owing to different factors such as infection, surgery, bacterial activities in dental plaques, and acidic food consumption [47–49]. For instance, in the presence of pathological diseases, the pH of the oral cavity can decrease to a value within the 2.0–3.0 range [50,51]. Nevertheless, it is the excellent corrosion resistance exhibited by HEAs that makes them attractive for biomedical applications [46]. Thus, some scientific work has already been undertaken in order to evaluate the corrosion resistance of the HEAs under conditions that simulate the aggressive environment provided by the human body [52–55]. The current work aims to contribute to this line of research and focuses on the investigation of corrosion behavior of HEAs in physiological media simulating blood (i.e. simulated body fluid (SBF)) and oral cavity (i.e. artificial saliva (AS)).

Notably, different elemental compositions of HEAs have been improved with the addition of Ti due to its high biocompatibility and high strength. For instance, some studies on the corrosion behavior of Ti-based HEAs showed superior resistance exhibited by these alloys as compared to traditionally used biomaterials, such as Ti–6Al–4V [52], against aggressive environments such as phosphate buffer saline (PBS), NaCl infusion solution, and simulated body solution [52–54]. Specifically, Ti–Ta-Hf alloy system was modified by addition of non-toxic late transition elements, such as Nb, Zr and Mo, [10,15,56,57] to provide enhanced biocompatibility, and TiTaHfNb, TiTaHfNbZr and TiTaHfMoZr HEAs were prepared and studied in this work. To the best of the authors' knowledge, the current work constitutes the first study focusing on the corrosion response of these HEA systems to assess their potential use in cardiovascular or oral implants in their bulk form.

Recent studies on one of Ti–Ta-Hf based alloys, namely TiTaHfNbZr alloy, showed that TiTaHfNbZr serves as an effective coating material when deposited on NiTi and Ti–6Al–4V substrates [13,58,59]. In particular, TiTaHfNbZr coating provided superior wear and corrosion resistance in aggressive physiological environments, encouraging further assessment of this particular HEA and its derivatives as biomaterials. The current study focuses on the TiTaHfNb, TiTaHfNbZr and TiTaHfMoZr HEAs in their as-cast form in order to evaluate their corrosion behavior in bulk form rather than as a coating on another metal substrate, such that their utility as an independent biomaterial can be assessed. For this purpose, bulk TiTaHfNb, TiTaHfNbZr and TiTaHfMoZr samples were subjected to static biocompatibility experiments in SBF and AS, and both samples and the immersion fluids underwent a thorough experimental examination in order to reveal the corrosion behavior of these materials. The key finding is that the TiTaHfNbZr alloy exhibited superior corrosion resistance in both SBF and AS, while the TiTaHfMoZr HEA sustained the most corrosion damage among all three alloys, and the TiTaHfNb alloy could not tolerate the SBF environment well. Overall, the findings presented and detailed in the remainder of this paper demonstrate the considerable corrosion resistance of these three HEAs, yet also warrant further investigation to uncover their potential use as biomaterials.

Table 1
Compositions of the AS and SBF utilized in the static immersion experiments.

Solution	Ingredients	Amount (g/L)	pH
AS	NaCl	0.4	2.3
	KCl	0.4	
	$CaCl_2{\cdot}2H_2o$	0.906	
	$NaH_2PO_4.2H_2O$	0.69	
	$Na_2S.9H_2O$	0.005	
	Urea	1	
SBF	NaCl	8.036	7.4
	$NaHCO_3$	0.352	
	KCL	0.225	
	$K_2HPO_4.3H_2O$	0.23	
	$MgCl_2.6H_2O$	0.311	
	1 M HCL	40 mL	
	$CaCl_2{\cdot}2H_2o$	0.293	
	Na_2SO_4	0.072	
	TRIS	6.063	
	1 M HCL	0.2 mL	

2. Experimental procedures

The HEAs studied in this work were synthesized by arc melting with a purity of 99.9%: the TiTaHfNb HEA was composed of 50 wt% Ti, 16.67 wt% Ta, 16.67 wt% Hf and 16.67 wt% Nb, whereas the TiTaHfNbZr and TiTaHfMoZr compositions were equimolar. The disc-

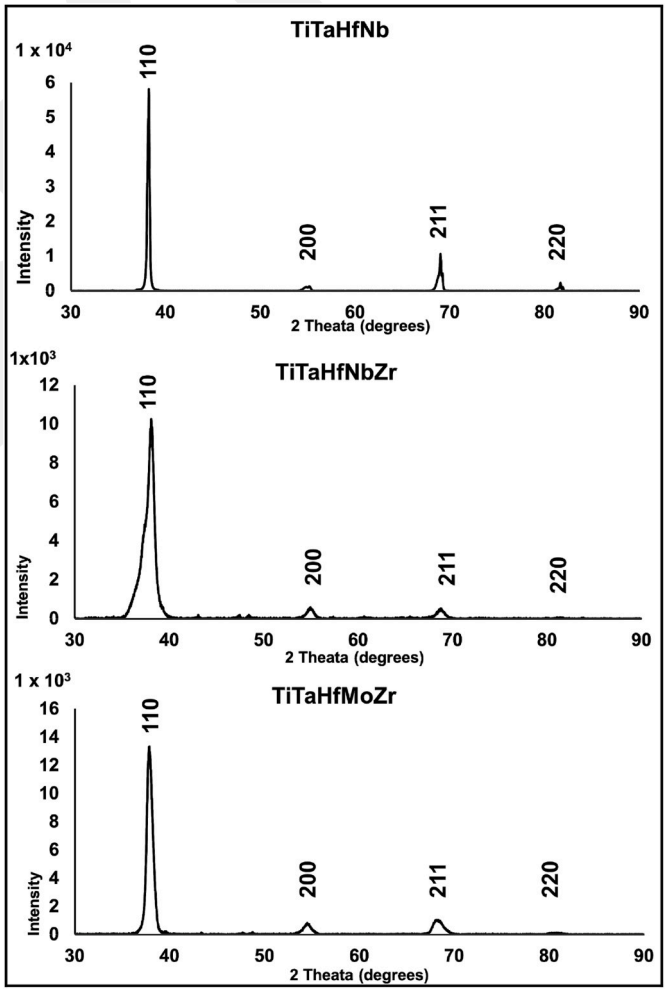

Fig. 1. XRD results of as-cast (a) TiTaHfNb, (b) TiTaHfNbZr, and (c) TiTaHfMoZr HEAs.

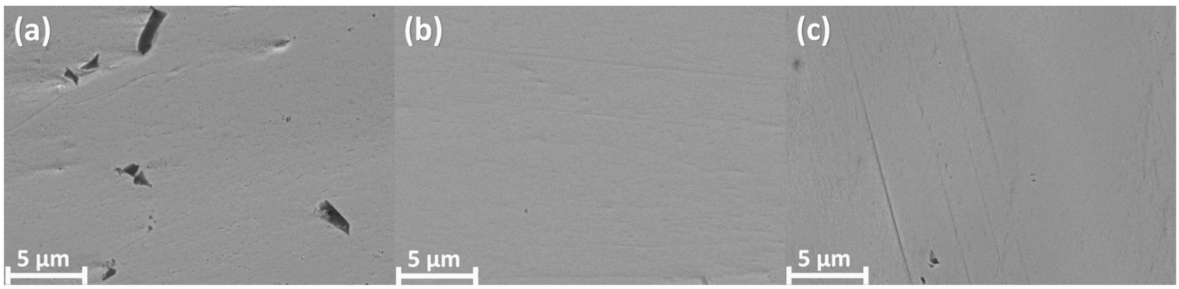

Fig. 2. The SEM images of the untested (a) TiTaHfNb, (b) TiTaHfNbZr and (c) TiTaHfMoZr sample surfaces following polishing.

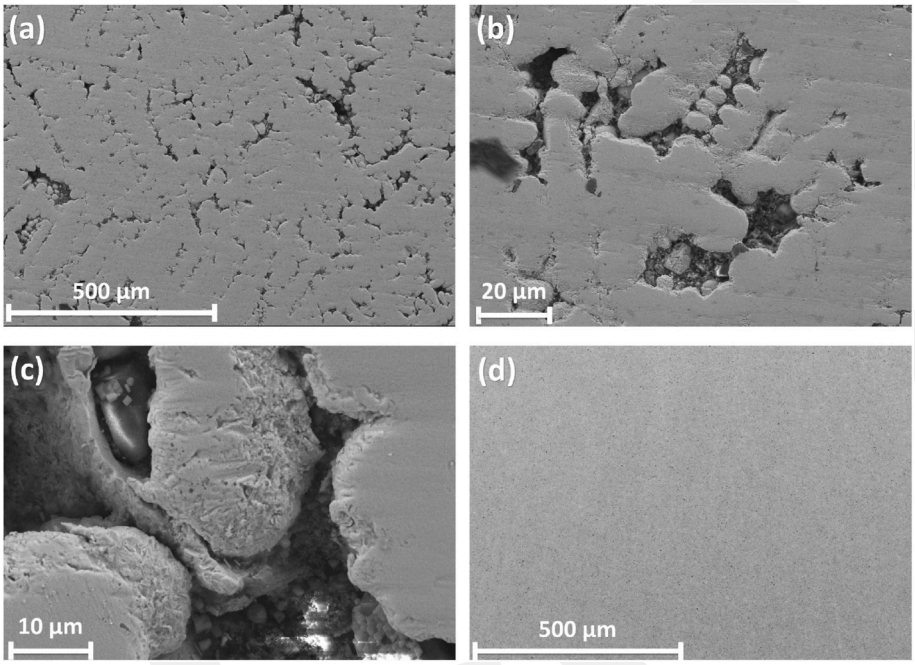

Fig. 3. SEM micrographs of the bulk TiTaHfNb sample surfaces following immersion for 28 days - (a), (b), (c): SBF, and (d): AS.

shaped multi-component alloys with a diameter of 50.1 mm and a thickness of 6.1 mm were cut by electrical discharge machining (EDM) to extract 10 mm × 5 mm x 1 mm bulk samples. Contaminations and EDM residue on the bulk sample surfaces were eliminated by mechanical polishing (without any change or with only negligible change in thickness of the samples). SiC emery papers with various grain sizes ranging from 106 to 2.5 µm were used, followed by polishing with 0.30 µm alumina slurry until the sample surfaces had mirror-like appearance. The bulk samples were cleaned with ethanol and rinsed with de-ionized water. After the cleaning procedure, the bulk samples were immersed into SBF (pH = 7.4) and AS (pH = 2.3) for 1, 7, 14 and 28 days. The solutions were kept at a constant temperature of 37 °C throughout the immersion with the aid of an electronically controlled water bath.

The composition of AS and SBF are provided in Table 1 [60]. Each HEA sample was immersed separately in a sealed tube, and the tubes were filled with the solutions, where a volume per surface area ratio of 20 mL/cm^2 was arranged [61]. The mass of each bulk sample was recorded before and after the immersion test to detect mass gain or loss by corrosion. Crystallographic identification of the alloys was accomplished by X-ray diffraction (XRD) method on a Bruker D2 Advanced X-ray diffractometer with a Cu-Kα radiation source operated at 30 kV and 10 mA. The incidence angle was about 5° and the acquisition angle ranged from 5° to 90°, where each step was processed with a 0.02° increment. The surface morphology of both untested and tested samples was investigated by a Zeiss Ultra Plus field emission scanning electron microscope (SEM). Ion release from the bulk samples into the immersion fluids was monitored using an Agilent 7700x inductively coupled plasma mass spectrometer (ICP-MS). A Thermo-Scientific K-Alpha X-Ray Photoelectron Spectrometer (XPS) were utilized to obtain chemical content information of from the surface of the samples after immersion tests.

3. Results and discussion

The XRD patterns of the as-cast TiTaHfNb, TiTaHfNbZr and TiTaHfMoZr alloys are provided in Fig. 1. Accordingly, the TiTaHfNb, TiTaHfNbZr and TiTaHfMoZr HEAs all consist of a single BCC phase, and the corresponding lattice parameters are 3.329 Å, 3.340 Å and 3.362 Å, respectively, where the peak values were calculated using Bragg's Law. Despite the very limited number of studies on the TiTaHfNb, TiTaHfNbZr and TiTaHfMoZr HEAs, the experimentally determined lattice parameters and the peak values are consistent with the literature to this point [55,62–64].

Surface morphology of the bulk HEAs before the immersion experiments were analyzed by SEM, revealing that TiTaHfNb, TiTaHfNbZr and TiTaHfMoZr had a smooth surface prior to immersion tests (Fig. 2). However, as seen in Fig. 3 (a), (b) and (c), the SEM micrographs of the TiTaHfNb demonstrate a highly corroded surface following 28 days immersion in SBF. Fig. 3 (a), (b), and (c) show that TiTaHfNb was negatively affected from the SBF environment and the locally intense

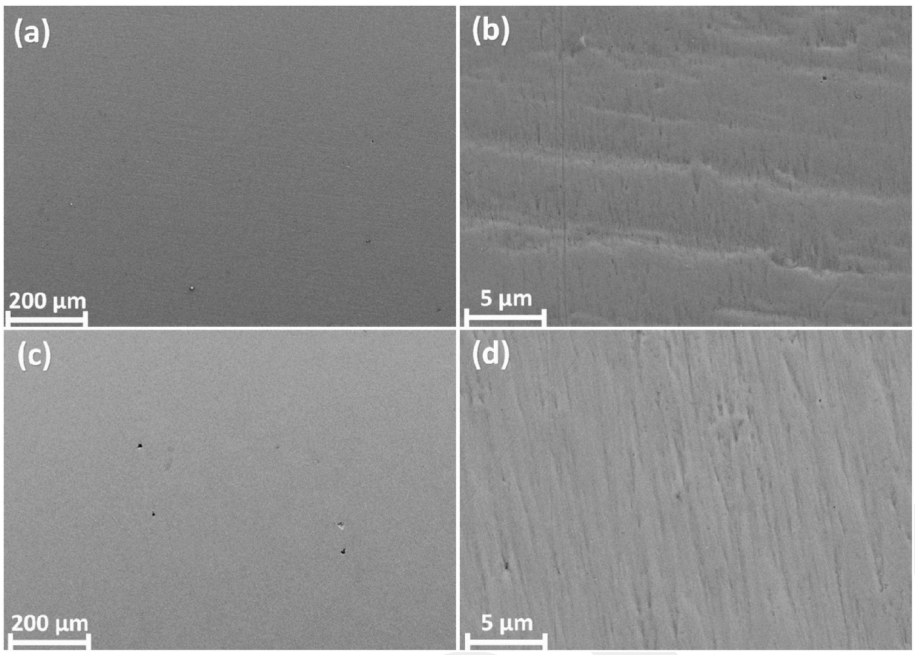

Fig. 4. SEM micrographs of the bulk TiTaHfNbZr sample surfaces following immersion for 28 days – (a), (b): SBF; (c) and (d): AS.

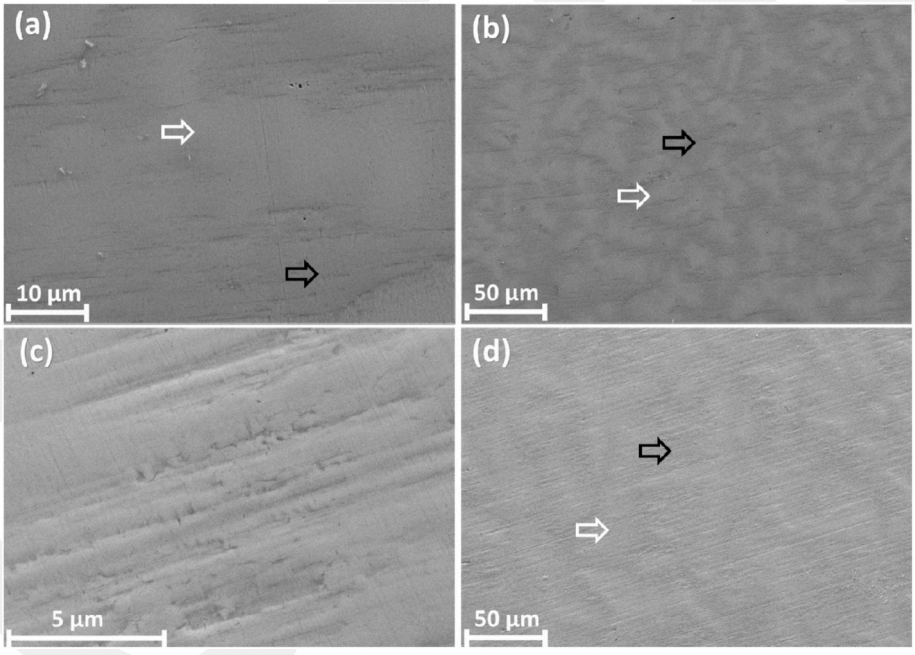

Fig. 5. SEM micrographs of the bulk TiTaHfMoZr sample surfaces following immersion for 28 days – (a), (b): SBF; (c) and (d): AS. Black arrows at (a), (b) and (d) indicate darker regions; white arrows indicate brighter regions.

corrosion behavior leads to enlargement of the corrosion through the thickness as indicated in Fig. 3 (b) and (c), which may result in pitting corrosion in long term applications. Indeed, several studies support the idea that sulphate and chloride ions present in SBF have significant effects on the corrosion behavior of metallic materials [53,65–69]. Specifically, existence of chloride ions could accelerate corrosion with the condition of delicate passivation layer. During corrosion process chloride ions can easily penetrate through the thin layer, giving way to pitting corrosion [53,65]. Besides, on TiTaHfNb sample surfaces, the vertically advancing corrosion behavior created ditch like structures and holes as can be seen in Fig. 3 (b) and (c). Therefore, it can be argued that the chloride ions facilitate pitting corrosion, and sulphate ions further worsen the corrosion by expanding the pits [69]. Consequently, TiTaHfNb cannot tolerate SBF environment since the experimental findings clearly indicate pitting corrosion. On the other hand, AS provides a more suitable environment for TiTaHfNb alloy, as evident from the lack of a substantially deformed surface that formed when immersed in SBF (Fig. 3 (d)). This significant difference between the surfaces of TiTaHfNb samples immersed in SBF and AS can be clearly seen in Fig. 3 (a) and (d). The smoother surface seen in (d) suggests higher corrosion resistance of TiTaHfNb against AS than SBF. After all, better surface response to AS was observed in TiTaHfNb despite the lower pH degree of AS.

As compared to the TiTaHfNb alloy, the TiTaHfNbZr HEA exhibited a

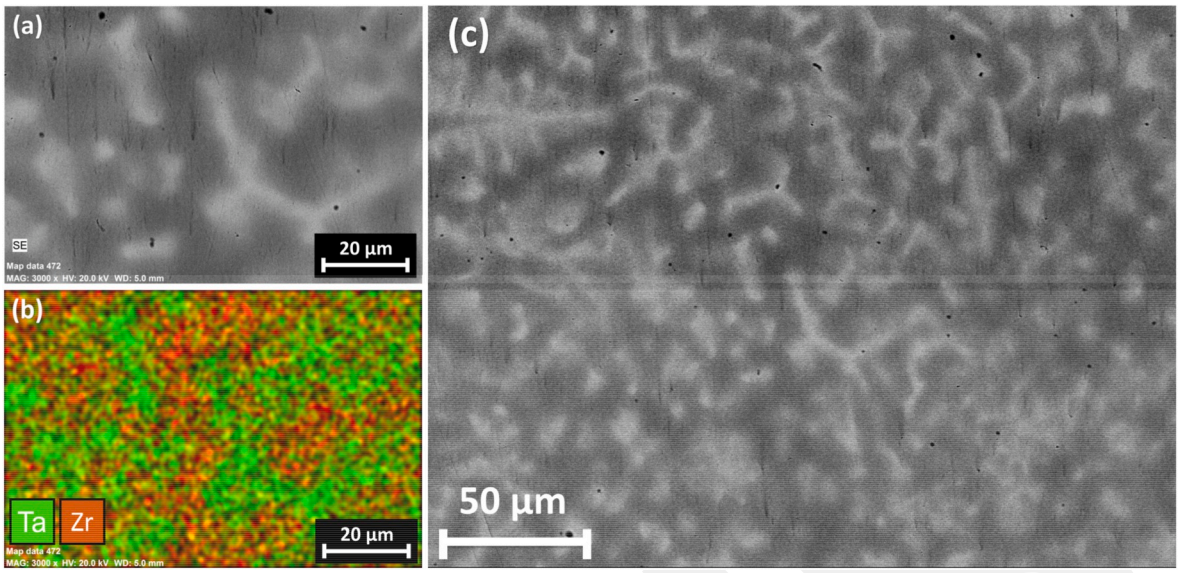

Fig. 6. EDX analysis results of the as-received TiTaHfMoZr sample: (a) nonhomogenous surface of TiTaHfMoZr, (b) EDX of TiTaHfMoZr surface. Green regions represent Ta-rich areas, and red regions represent Zr-rich areas; (c) BSE image of the nonhomogenous region. (For interpretation of the references to color in this figure legend, the reader is referred to the Web version of this article.)

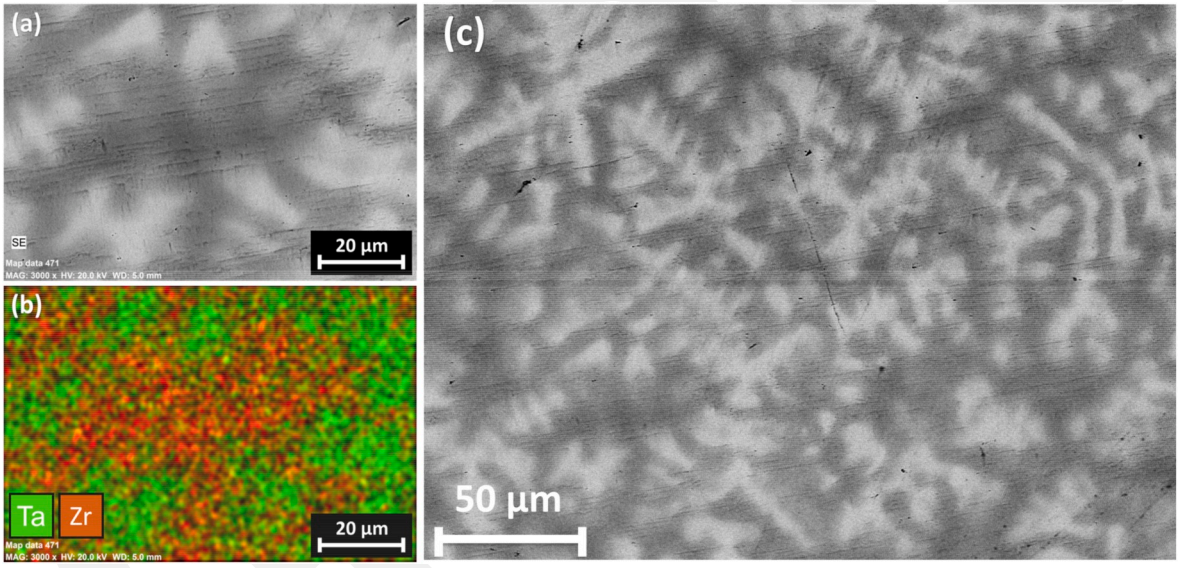

Fig. 7. EDX analysis results of the TiTaHfMoZr sample following 28 days of immersion in SBF: (a) nonhomogenous surface of TiTaHfMoZr, (b) EDX of TiTaHfMoZr surface; Green regions represent Ta-rich areas, and red regions represent Zr-rich areas; (c) BSE image of the nonhomogenous region. (For interpretation of the references to color in this figure legend, the reader is referred to the Web version of this article.)

more stable behavior in both SBF and AS: as shown in Fig. 4, there is no significant corrosion on the surface of the TiTaHfNbZr following immersion in SBF and AS, and the material highly resists to both these aggressive environments with negligible amount of corrosion. In contrast to TiTaHfNbZr, non-homogeneous degradation prevailed on the surface of TiTaHfMoZr due to significant amount of Mo ion release. Two distinct regions were recognized prior to immersion and following 28 days of immersion in SBF and AS, as evident from the SEM micrographs in Fig. 5 and back scattered electron (BSE) images presented in Figs. 6 and 7. These two regions were analyzed by EDX and in BSE mode (Figs. 6 and 7), which coexist as a consequence of nonhomogeneous distribution of the components during solidification process that lead to dendritic structures [25]. The dendritic regions consist of heavier elements as Ta-rich areas were observed within darker regions, which are Zr-rich. However, XRD pattern of the TiTaHfMoZr HEA reveals its single BCC phase (Fig. 1(c)): while the segregation tendency leads to formation of Ta-rich areas, the single BCC-phase formed during solidification, such that there is a negligible difference between the lattice parameters of the dendritic and inter-dendritic phases [70].

As illustrated in Fig. 6 (a) and (b), and 7 (a) and (b), dendrites indicate Ta-rich areas with a higher melting point, leading to earlier crystallization [71], and Zr-rich areas dominated the inter-dendrite regions. This inhomogeneous elemental distribution was brought about by the addition of Mo, which presents long "*hands-on*" time that leads to low reduced-activity application during manufacturing process [70]. On the other hand, TiTaHfMoZr showed better corrosion resistance in SBF environment. The difference between corroded surfaces induced by SBF and AS are apparent from Fig. 5 (a) and (c), such that AS induced more damage to the surface of TiTaHfMoZr. Thus, one can conclude that TiTaHfMoZr performs better in SBF than in AS. Moreover, more ion

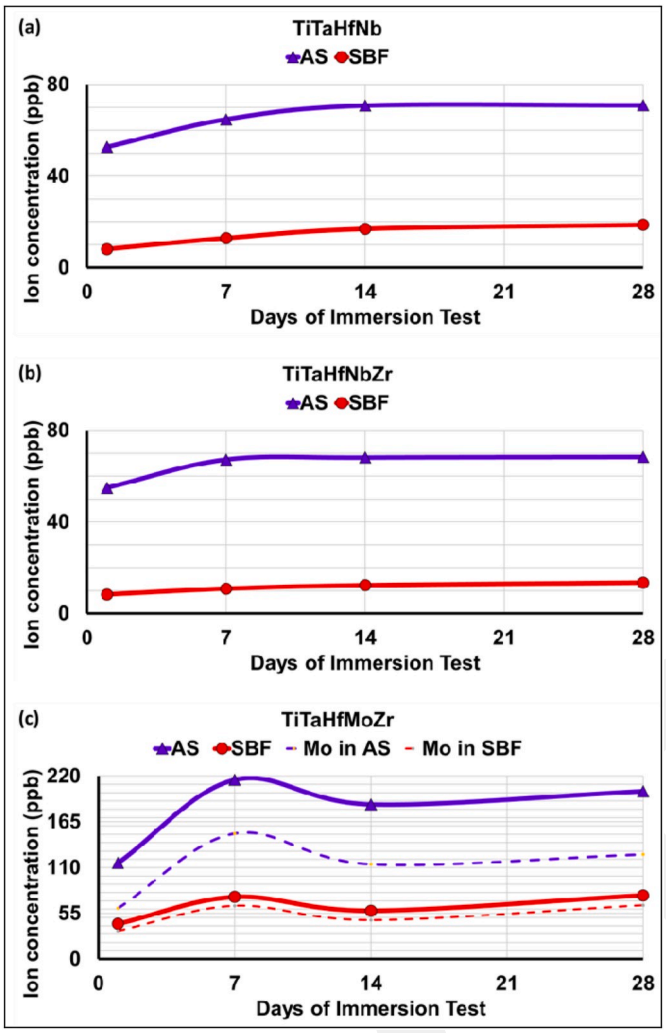

Fig. 8. Total ion concentrations of (a) Ti, Ta and Nb released from TiTaHfNb; (b) Ti, Ta, Nb and Zr released from TiTaHfNbZr; and (c) Ti, Ta, Mo and Zr released from TiTaHfMoZr. The dashed lines represent released Mo ion concentration upon immersion in SBF and AS following 1, 7, 14 and 28 days. Note that the total ion concentration does not include Hf concentration due to its insignificant amount.

release from the Zr-rich inter-dendritic phases was prevalent: Specifically, the preferred corrosion of inter-dendritic phase over the dendritic phase can be attributed to different chemical composition of the dendrites, such that the enhanced dissolution stems from the higher electropositivity of the Zr-rich regions [72].

It should be noted that the low pH value of AS, which represents an extremely acidic oral cavity in case of any inflammations or metabolic activities, has a significant ionization effect on all three HEAs as evidenced by the surface degradation. SEM micrographs (Figs. 4 and 5) demonstrate the aggressive nature of AS and the corresponding corrosion damage it causes, while supporting data from the ICP-MS experiments (Fig. 8) demonstrate the negative impact of AS on the ion release behavior of the studied HEAs: the amount of total ion release form all three HEAs was much higher in AS at the end of the 28th day as compared to the SBF.

As illustrated in Fig. 8, SBF and AS contain very similar levels of ion concentrations after immersion of TiTaHfNb and TiTaHfNbZr samples, however; addition of Zr enhances corrosion resistance, such that TiTaHfNbZr shows better protection against ion release, as evidenced by the less total ion release from TiTaHfNbZr (as compared to TiTaHfNb) following the 1st week of immersion in both media. The highest total released ion concentrations in SBF and AS were obtained from the immersion tests of TiTaHfMoZr (Fig. 8). TiTaHfMoZr showed almost 5 and 3 times more ion release into the SBF and AS, respectively, while relatively small quantity of ions was released from the TiTaHfNb and TiTaHfNbZr. This significantly enhanced ion release behavior from the former HEA is attributed to Mo replacing Nb in the other two materials: apparently, Nb acts as a stabilizer and restricts the quantity of released ions from the bulk [54,73,74].

On the other hand, cyclically repeated elemental release implies a passive layer formation and dissolution over specific time periods [75,76]. Specifically, the total ion release from TiTaHfMoZr increased within the first 7 days, and then decreased until the 14th day, followed by an increased ion concentration up until the end of the 28th day (Fig. 8). Consequently, the observed trend between the total ion release (Fig. 8) is remarkable and clearly evidences the formation-dissolution cycle of a passive surface layer.

In order to clarify this ambiguity, samples expected to form a passive oxide layer were analyzed with XPS. TiTaHfNb, TiTaHfNbZr and TiTaHfMoZr were significantly exposed to corrosion in AS without highly corroded surface properties observed by SEM in Figs. 3–5, such that the results of ICP-MS led to the investigation of the possibility of a passive oxide layer formation. Therefore, elemental compositions of TiTaHfNb, TiTaHfNbZr and TiTaHfMoZr samples following 28 days of immersion in AS were analyzed by XPS. The samples were initially etched for 60 s to eliminate organic impurities, then the etching process was continued until 3000 s for the TiTaHfNb, TiTaHfNbZr and TiTaHfMoZr samples. XPS analysis results proved that TiTaHfNb, TiTaHfNbZr and TiTaHfMoZr formed a passive oxide layer on their surfaces following a 28-day immersion test in AS, and oxides of Ti,Ta,Hf,Nb, Mo and Zr were found on the surfaces of the HEAs during the post-mortem investigation. It should be noted that the XPS analysis focused on Zr and its oxides, mainly because Zr has ability to form a strong and adherent passive layer on a material surface [77,78]. As illustrated in Fig. 9, while both materials have oxygen on their surfaces, the amount of oxygen decreases and the amount of metal increases concomitant with the distance from the surface. As etching moves from the surface to deeper layers, oxygen is replaced by metal oxide, which is eventually replaced by pure metal elements, as can be seen in Figs. 9 and 10.

The XPS results showed that oxide layer formation exist for the HEAs in both of SBF and AS. However, the higher amount of ion release from the HEAs in AS has been observed from the ICP-MS results (Fig. 8), such that it is preferred to illustrate the XPS results of the HEAs after immersed in AS in order to observe oxide layer formation clearly. Even though TiTaHfNb, TiTaHfNbZr and TiTaHfMoZr HEAs exhibited higher ion release in AS (pH = 2.4) than in SBF (Fig. 8), a healthier (smoother) surface appearance was noted following the immersion tests in AS with negligible surface degradations as evidenced from SEM images (Fig. 3 (d)); Fig. 4 (c) and (d); Fig. 5 (c) and (d)). This is attributed to the surface layer formation, such that passive layer forming on the surface covers the surface deteriorations initially induced by the corrosion. Examination of the XPS results for TiTaHfNbZr and TiTaHfMoZr (Fig. 9 (a) and (b)) reveals that oxygen and Zr-oxides predominantly exist on the surface up to 300 s etch time, and Zr-metal appears with further etching. The XPS spectra of the O 1s and Zr 3d peaks are indicated in Fig. 9 for the 28-day-immersed TiTaHfNbZr and TiTaHfMoZr in AS to observe layer properties on the bulk surfaces. The peak of the O 1s profile as shown in Fig. 9(c) is located at 530.6 eV binding energy (BE) for TiTaHfNbZr, and 530.9 eV and 530.6 eV BE are the peaks for 0 s etch time and 900 s etch time of TiTaHfMoZr, respectively (Fig. 9(d)). The O 1s peak locations agree well with the depth profiles (Fig. 9 (a) and (b)), such that oxygen content prevails on the surface of both HEAs, and the content decreases going from the surface to deeper into the bulk. The Zr 3d spectra shown in Fig. 9 have doublet peaks of $3d_{5/2}$ and $3d_{3/2}$ due to spin-orbit-split [79], and the energy difference between the doublets is 2.4 eV [80]. Four doublets (the couples of $Zr3d_{3/2}$ and $Zr3d_{5/2}$) have been obtained from the XPS results that can be attributed to four different types of BE of

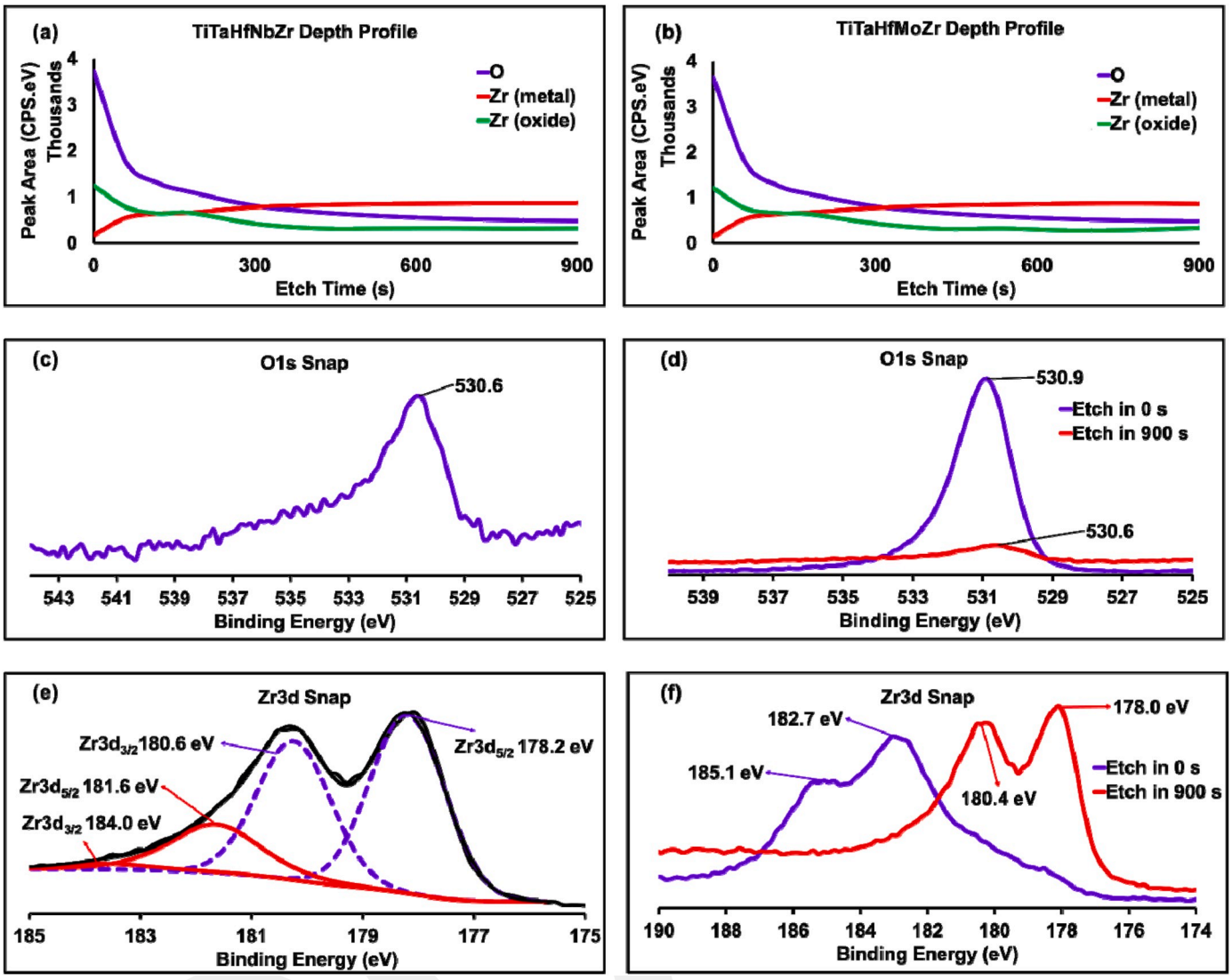

Fig. 9. XPS depth profiles of (a) TiTaHfNbZr and (b)TiTaHfMoZr; oxygen peaks of (c) TiTaHfNbZr and (d) TiTaHfMoZr; Zr and ZrO_2 peaks of (e) TiTaHfNbZr and (f) TiTaHfMoZr.

Zr-metal, Zr-oxide and Zr-sub oxides as illustrated in Fig. 9(e)) [80,81]. The peaks at 178.2 eV and 180.6 eV binding energy corresponding to Zr $3d_{5/2}$ and Zr $3d_{3/2}$, respectively, indicate the presence of metallic Zr (Fig. 9(e)), as these peaks are consistent with previously reported binding energies of metallic Zr are 178.8 eV [82,83] and 177.93 eV [84] for Zr $3d_{5/2}$; and 180.33 eV [84] for Zr $3d_{3/2}$. On the other hand, 184.0 eV (Zr $3d_{5/2}$) and 181.6 eV (Zr $3d_{3/2}$) peaks (Fig. 9 (e)) strongly point out to the existence of oxide layer formation on the TiTaHfNbZr surface following 28 days immersion in AS. These peaks are close to the binding energy of ZrO_2 that has been reported as 184.3 eV and 181.9 eV corresponding to Zr $3d_{5/2}$ and Zr $3d_{3/2}$, respectively [85]; and 183.7 eV and 181.3 eV for Zr-oxide (Zr^{+2}) [80], and 186.60 eV [86,87] for ZrO_2.

The relationship between etch time and surface layer properties is presented in Fig. 9(f). The peaks are centered at 182.7 eV BE and 185.1 eV BE that agree with the oxide layer formation on TiTaHfMoZr surface following 28 days of immersion in AS, and these peaks are close to the binding energies reported in literature: some studies reported peak values of Zr-oxide (Zr^{3+}) as 182.6 eV and 185.0 eV [80]; and 182.66 eV and 185.06 eV [84], corresponding to Zr $3d_{5/2}$ and Zr $3d_{3/2}$, respectively. Consequently, the XPS results confirmed the existence of Zr-oxide film on the surface of the HEAs. Moreover, Ti-oxide formation on the HEAs surface was investigated by XPS following the immersion tests in SBF and AS. The XPS results indicate Ti-oxide formation on the TiTaHfNb HEA surface following 28-days immersion in AS (Fig. 10(a)), however; there is no indication of Ti-oxide on TiTaHfNb, TiTaHfNbZr, and TiTaHfMoZr following 28-days of immersion in SBF; and on TiTaHfNbZr, and TiTaHfMoZr following 28 days of immersion in AS. The XPS results of the HEA samples immersed in AS are illustrated in Fig. 10: Ti-oxide was observed on TiTaHfNb surface following 28-days immersion, as evidenced by the higher peak points at etch time 0 s (Fig. 10 (a)) as compared to the peaks at the etch time 1080 s in Fig. 10 (b). Moreover, the doublet peaks of Ti2p spectra in Fig. 10(a) are assigned to Ti-oxide formation: for instance, in the case of TiTaHfNb immersed in AS the peak of $Ti2p_{3/2}$ is located at 458.9 eV at etch time 0 s (Fig. 10(a)), which is attributed to Ti^{+4} on the TiTaHfNb surface and is consistent with the literature [88–90]. In comparison, 453.6 eV of binding energy is prevalent for $Ti2p_{3/2}$ at 1080 s etching time (Fig. 10 (b)), indicating the presence of metallic Ti consistent with the literature [90,91]. Consequently, one can conclude that Ti-oxide coexists with the other metallic oxides such as Zr-oxide on the TiTaHfNb HEA surface, while the metallic Ti prevails at the deeper layers (Fig. 10 (a) and (b)). On the other hand, the Ti2p doublets with the binding energies of $Ti2p_{3/2}$, namely 453.3 eV and 453.5 eV for TiTaHfNbZr, and 453.7 eV and 453.8 eV for TiTaHfMoZr, are consistent with the peaks of metallic

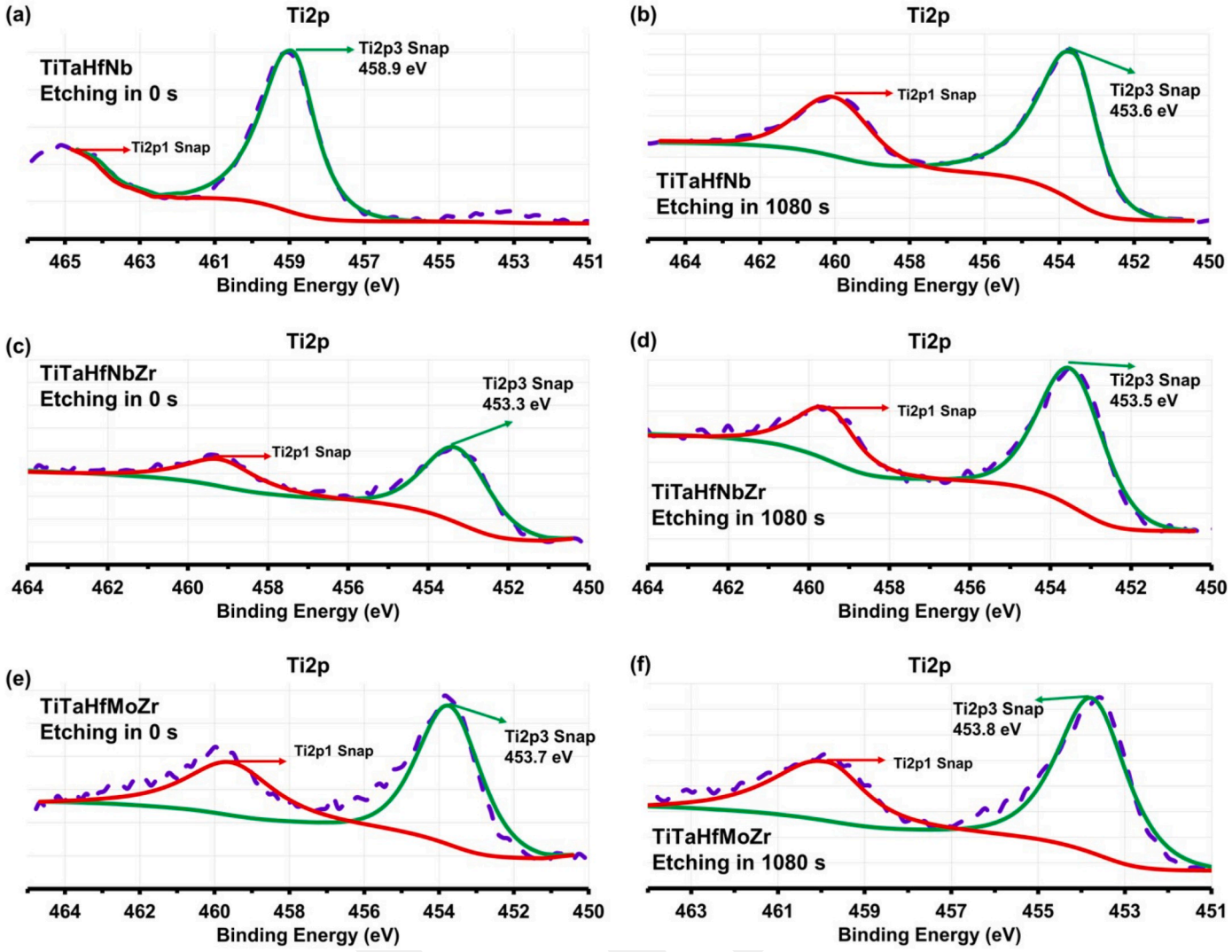

Fig. 10. XPS results of TiTaHfNb immersed in AS for 28 days: (a) for etch time 0 s, (b) for etch time 1080 s; TiTaHfNbZr immersed in AS for 28 days: (c) for etch time 0 s, (d) for etch time 1080 s; and TiTaHfMoZr immersed in AS for 28 days: (e) for etch time 0 s, (f) for etch time 1080 s.

Ti reported in literature [90,91]. Consequently, Ti-oxide contributes to the oxide layer forming on the TiTaHfNb HEA surface following the 28 days of immersion in AS, which, however; was not the case for TiTaHfNbZr and TiTaHfMoZr immersed in AS, or TiTaHfNb, TiTaHfNbZr and TiTaHfMoZr immersed in SBF. Overall, these findings indicate the formation of a more stable Zr-oxide layer on all HEA surfaces immersed in both AS and SBF, and an additional Ti-oxide formation on TiTaHfNb immersed in AS.

This passive film formation is supported by XPS results presented in Figs. 9 and 10, as well as the XRD results provided in Fig. 11. The XRD results indicated that TiTaHfNbZr shows lower intensity peaks (Fig. 11): the Zr addition to TiTaHfNb accelerates the formation of passive layer, leading to an amorphous layer. As for the TiTaHfMoZr HEA, it exhibited higher peak intensity than the TiTaHfNbZr alloy, which can be attributed to possible Mo precipitation and nonhomogeneous structure of TiTaHfMoZr (Figs. 5–7). This passive layer formation on TiTaHfNb, TiTaHfNbZr and TiTaHfMoZr supported by the current SEM micrographs, ICP-MS results, XPS results and the XRD data suggests that these TiTaHf-based HEAs can sustain long-term corrosion resistance, which, however; should be studied in detail before drawing any conclusions regarding their biomedical utility.

4. Conclusions

Corrosion response of three TiTaHf-based HEAs, namely TiTaHfNb, TiTaHfNbZr and TiTaHfMoZr, was inspected employing static immersion experiments in simulated body fluid (SBF) and artificial saliva (AS) in order to assess the potential biomedical utility of these alloys. As a result of immersion experiments that were carried out for periods of 1, 7, 14 and 28 days, the TiTaHfNb HEA was observed to suffer from pitting corrosion in SBF, while it exhibited a healthier surface following immersion in AS. The presence of Zr and Nb in the samples were observed to enhance corrosion performance with reduced ion release and better surface properties as evidenced by the results of the TiTaHfNbZr test results. On the contrary, Mo addition resulted in an inhomogeneous microstructure (TiTaHfMoZr), leading to dendrite structures and significant amount of ion release upon immersion in both media. In addition, XPS and XRD results along with the ICP-MS ion release trends showed that a passive layer formation was present on all HEA surfaces, implying that corrosion resistance can be sustained in long-term applications. Overall, the set of findings presented herein demonstrate the potential of the TiTaHf-based HEAs to be utilized as implant materials, but also warrant a more detailed analysis of these materials before drawing any conclusions.

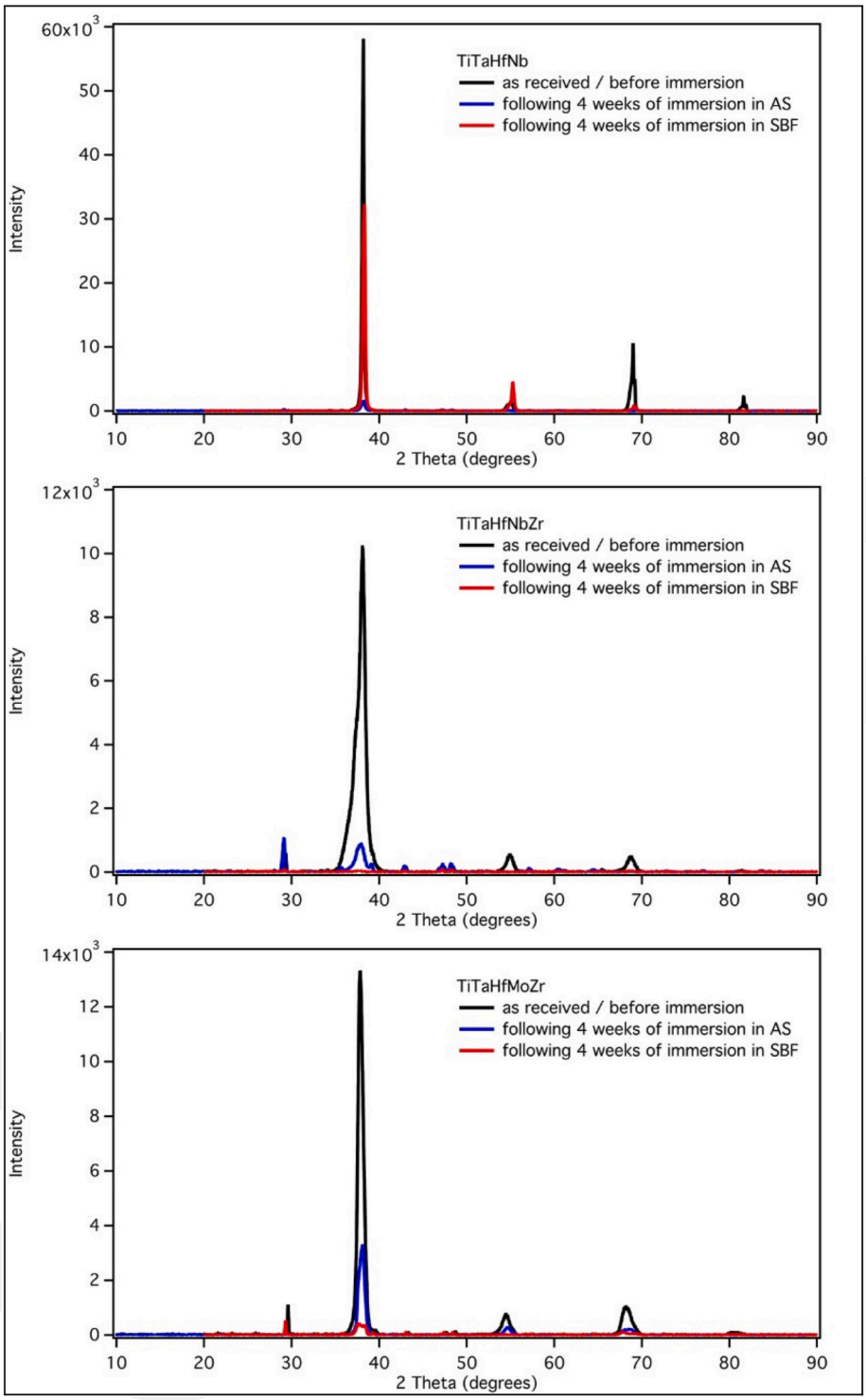

Fig. 11. XRD scans of TiTaHfNb, TiTaHfNbZr and TiTaHfMoZr prior to and following the immersion experiments.

Declaration of competing interest

This is an original paper which has neither previously, nor simultaneously, in whole or in part been submitted to or published anywhere else. The article has been written by the stated authors who are all aware of its content and approve its submission. Furthermore, the authors claim no conflict of interest, and if accepted, the article will not be published elsewhere in the same form, in any language, without the written consent of the publisher.

CRediT authorship contribution statement

S. Gurel: Formal analysis, Methodology, Writing - original draft. **M. B. Yagci:** Formal analysis, Methodology, Writing - original draft. **B. Bal:** Writing - original draft. **D. Canadinc:** Writing - original draft, Supervision.

Acknowledgments

This work was supported by the BAGEP Award of the Science

Academy. B. Bal acknowledges the AGU-BAP [grant number FAB-2017-77].

References

[1] D.F. Williams, On the mechanisms of biocompatibility, Biomaterials 29 (2008) 2941–2953, https://doi.org/10.1016/j.biomaterials.2008.04.023.

[2] D.F. Williams, On the nature of biomaterials, Biomaterials 30 (2009) 5897–5909, https://doi.org/10.1016/j.biomaterials.2009.07.027.

[3] W. Jin, P.K. Chu, Orthopedic implants, in: Encycl. Biomed. Eng, Elsevier, 2019, pp. 425–439, https://doi.org/10.1016/B978-0-12-801238-3.10999-7.

[4] M. Geetha, A.K. Singh, R. Asokamani, A.K. Gogia, Ti based biomaterials, the ultimate choice for orthopaedic implants – a review, Prog. Mater. Sci. 54 (2009) 397–425, https://doi.org/10.1016/j.pmatsci.2008.06.004.

[5] M.P. Staiger, A.M. Pietak, J. Huadmai, G. Dias, Magnesium and its alloys as orthopedic biomaterials: a review, Biomaterials 27 (2006) 1728–1734, https://doi.org/10.1016/j.biomaterials.2005.10.003.

[6] M. Niinomi, Recent metallic materials for biomedical applications, Metall. Mater. Trans. 33 (2002) 477–486, https://doi.org/10.1007/s11661-002-0109-2.

[7] Q. Chen, G.A. Thouas, Metallic implant biomaterials, Mater. Sci. Eng. R Rep. 87 (2015) 1–57, https://doi.org/10.1016/j.mser.2014.10.001.

[8] F. Rupp, J. Geis-Gerstorfer, K.E. Geckeler, Dental implant materials: surface modification and interface phenomena, Adv. Mater. 8 (1996) 254–257, https://doi.org/10.1002/adma.19960080316.

[9] U. Kamachimudali, T.M. Sridhar, B. Raj, Corrosion of bio implants, Sadhana 28 (2003) 601–637, https://doi.org/10.1007/BF02706450.

[10] M. Niinomi, M. Nakai, J. Hieda, Development of new metallic alloys for biomedical applications, Acta Biomater. 8 (2012) 3888–3903, https://doi.org/10.1016/j.actbio.2012.06.037.

[11] C. Lhotka, T. Szekeres, I. Steffan, K. Zhuber, K. Zweymüller, Four-year study of cobalt and chromium blood levels in patients managed with two different metal-on-metal total hip replacements, J. Orthop. Res. 21 (2003) 189–195, https://doi.org/10.1016/S0736-0266(02)00152-3.

[12] Y. Song, D.S. Xu, R. Yang, D. Li, W.T. Wu, Z.X. Guo, Theoretical study of the effects of alloying elements on the strength and modulus of β-type bio-titanium alloys, Mater. Sci. Eng. 260 (1999) 269–274, https://doi.org/10.1016/S0921-5093(98)00886-7.

[13] C.B. Aksoy, D. Canadinc, M.B. Yagci, Assessment of Ni ion release from TiTaHfNbZr high entropy alloy coated NiTi shape memory substrates in artificial saliva and gastric fluid, Mater. Chem. Phys. 236 (2019) 121802, https://doi.org/10.1016/j.matchemphys.2019.121802.

[14] C.-C. Shih, S.-J. Lin, Y.-L. Chen, Y.-Y. Su, S.-T. Lai, G.J. Wu, C.-F. Kwok, K.-H. Chung, The cytotoxicity of corrosion products of nitinol stent wire on cultured smooth muscle cells, J. Biomed. Mater. Res. 52 (2000) 395–403, https://doi.org/10.1002/1097-4636(200011)52:2<395::AID-JBM21>3.0.CO;2-B.

[15] Y. Yuan, Y. Wu, Z. Yang, X. Liang, Z. Lei, H. Huang, H. Wang, X. Liu, K. An, W. Wu, Z. Lu, Formation, structure and properties of biocompatible TiZrHfNbTa high-entropy alloys, Mater. Res. Lett. 7 (2019) 225–231, https://doi.org/10.1080/21663831.2019.1584592.

[16] C. Oldani, A. Dominguez, Titanium as a biomaterial for implants, in: Recent Adv. Arthroplast, InTech, 2012, https://doi.org/10.5772/27413.

[17] S. Rajendran, J. Paulraj, P. Rengan, J. Jeyasundari, M. Manivannan, Corrosion behaviour of metals in artificial saliva in presence of spirulina powder, J. Dent. Oral Hygiene 1 (1) (2009) 001–008.

[18] S.G. Steinemann, Metal implants and surface reactions, Injury 27 (1996), https://doi.org/10.1016/0020-1383(96)89027-9. S/C16-S/C22.

[19] R. Van Noort, Titanium: the implant material of today, J. Mater. Sci. 22 (1987) 3801–3811, https://doi.org/10.1007/BF01133326.

[20] Z. Tang, L. Huang, W. He, P. Liaw, Alloying and processing effects on the aqueous corrosion behavior of high-entropy alloys, Entropy 16 (2014) 895–911, https://doi.org/10.3390/e16020895.

[21] S.D. Cramer, B.S. Covino (Eds.), Corrosion: Fundamentals, Testing, and Protection, ASM International, 2003, https://doi.org/10.31399/asm.hb.v13a.9781627081825.

[22] B. Cantor, I.T.H. Chang, P. Knight, A.J.B. Vincent, Microstructural development in equiatomic multicomponent alloys, Mater. Sci. Eng. 375–377 (2004) 213–218, https://doi.org/10.1016/j.msea.2003.10.257.

[23] Y. Zhang, X. Yang, P.K. Liaw, Alloy design and properties optimization of high-entropy alloys, J. Occup. Med. 64 (2012) 830–838, https://doi.org/10.1007/s11837-012-0366-5.

[24] Y.F. Ye, Q. Wang, J. Lu, C.T. Liu, Y. Yang, Design of high entropy alloys: a single-parameter thermodynamic rule, Scripta Mater. 104 (2015) 53–55, https://doi.org/10.1016/j.scriptamat.2015.03.023.

[25] M. Todai, T. Nagase, T. Hori, A. Matsugaki, A. Sekita, T. Nakano, Novel TiNbTaZrMo high-entropy alloys for metallic biomaterials, Scripta Mater. 129 (2017) 65–68, https://doi.org/10.1016/j.scriptamat.2016.10.028.

[26] J.-W. Yeh, S.-K. Chen, S.-J. Lin, J.-Y. Gan, T.-S. Chin, T.-T. Shun, C.-H. Tsau, S.-Y. Chang, Nanostructured high-entropy alloys with multiple principal elements: novel alloy design concepts and outcomes, Adv. Eng. Mater. 6 (2004) 299–303, https://doi.org/10.1002/adem.200300567.

[27] L. Vinet, A. Zhedanov, A 'missing' family of classical orthogonal polynomials, J. Phys. A Math. Theor. 44 (2011), 085201, https://doi.org/10.1088/1751-8113/44/8/085201.

[28] W. Zhang, P.K. Liaw, Y. Zhang, Science and technology in high-entropy alloys, Sci. China Mater. 61 (2018) 2–22, https://doi.org/10.1007/s40843-017-9195-8.

[29] X.W. Qiu, Y.P. Zhang, L. He, C.G. Liu, Microstructure and corrosion resistance of AlCrFeCuCo high entropy alloy, J. Alloys Compd. 549 (2013) 195–199, https://doi.org/10.1016/j.jallcom.2012.09.091.

[30] Z.D. Han, H.W. Luan, X. Liu, N. Chen, X.Y. Li, Y. Shao, K.F. Yao, Microstructures and mechanical properties of Ti NbMoTaW refractory high-entropy alloys, Mater. Sci. Eng. 712 (2018) 380–385, https://doi.org/10.1016/j.msea.2017.12.004.

[31] T.-T. Shun, L.-Y. Chang, M.-H. Shiu, Microstructures and mechanical properties of multiprincipal component CoCrFeNiTix alloys, Mater. Sci. Eng. 556 (2012) 170–174, https://doi.org/10.1016/j.msea.2012.06.075.

[32] O.N. Senkov, J.M. Scott, S.V. Senkova, D.B. Miracle, C.F. Woodward, Microstructure and room temperature properties of a high-entropy TaNbHfZrTi alloy, J. Alloys Compd. 509 (2011) 6043–6048, https://doi.org/10.1016/j.jallcom.2011.02.171.

[33] X.F. Wang, Y. Zhang, Y. Qiao, G.L. Chen, Novel microstructure and properties of multicomponent CoCrCuFeNiTix alloys, Intermetallics 15 (2007) 357–362, https://doi.org/10.1016/j.intermet.2006.08.005.

[34] R. Sriharitha, B.S. Murty, R.S. Kottada, Alloying, thermal stability and strengthening in spark plasma sintered AlxCoCrCuFeNi high entropy alloys, J. Alloys Compd. 583 (2014) 419–426, https://doi.org/10.1016/j.jallcom.2013.08.176.

[35] Y. Qiu, M.A. Gibson, H.L. Fraser, N. Birbilis, Corrosion characteristics of high entropy alloys, Mater. Sci. Technol. 31 (2015) 1235–1243, https://doi.org/10.1179/1743284715Y.0000000026.

[36] Y. Qiu, S. Thomas, M.A. Gibson, H.L. Fraser, N. Birbilis, Corrosion of high entropy alloys, Npj Mater. Degrad. 1 (2017) 15, https://doi.org/10.1038/s41529-017-0009-y.

[37] B. Gludovatz, A. Hohenwarter, D. Catoor, E.H. Chang, E.P. George, R.O. Ritchie, ChemInform abstract: a fracture-resistant high-entropy alloy for cryogenic applications, ChemInform 45 (2014), https://doi.org/10.1002/chin.201447007 no-no.

[38] Z. Zhang, M.M. Mao, J. Wang, B. Gludovatz, Z. Zhang, S.X. Mao, E.P. George, Q. Yu, R.O. Ritchie, Nanoscale origins of the damage tolerance of the high-entropy alloy CrMnFeCoNi, Nat. Commun. 6 (2015) 10143, https://doi.org/10.1038/ncomms10143.

[39] Y.-J. Hsu, W.-C. Chiang, J.-K. Wu, Corrosion behavior of FeCoNiCrCux high-entropy alloys in 3.5% sodium chloride solution, Mater. Chem. Phys. 92 (2005) 112–117, https://doi.org/10.1016/j.matchemphys.2005.01.001.

[40] M.-H. Tsai, J.-W. Yeh, High-entropy alloys: a critical review, Mater. Res. Lett. 2 (2014) 107–123, https://doi.org/10.1080/21663831.2014.912690.

[41] C. Bauer, Recent studies on transport of respiratory gases by the red blood cell, Proc. Roy. Soc. Med. 68 (1975) 266–267, https://doi.org/10.1007/s11837-013-0761-6.

[42] C.J. Tong, M.R. Chen, S.K. Chen, J.W. Yeh, T.T. Shun, S.J. Lin, S.Y. Chang, Mechanical performance of the AlxCoCrCuFeNi high-entropy alloy system with multiprincipal elements, Metall. Mater. Trans. A Phys. Metall. Mater. Sci. (2005) 1263–1271, https://doi.org/10.1007/s11661-005-0218-9.

[43] N.N. Guo, L. Wang, L.S. Luo, X.Z. Li, Y.Q. Su, J.J. Guo, H.Z. Fu, Microstructure and mechanical properties of refractory MoNbHfZrTi high-entropy alloy, Mater. Des. 81 (2015) 87–94, https://doi.org/10.1016/j.matdes.2015.05.019.

[44] Y. Zhang, Y. Liu, Y.X. Li, X. Chen, H.W. Zhang, Microstructure and mechanical properties of a new refractory $HfNbSi_{0.5}TiVZr$ high entropy alloy, Mater. Sci. Forum 849 (2016) 76–84. https://doi.org/10.4028/www.scientific.net/MSF.849.76.

[45] C.-C. Juan, M.-H. Tsai, C.-W. Tsai, C.-M. Lin, W.-R. Wang, C.-C. Yang, S.-K. Chen, S.-J. Lin, J.-W. Yeh, Enhanced mechanical properties of HfMoTaTiZr and HfMoNbTaTiZr refractory high-entropy alloys, Intermetallics 62 (2015) 76–83, https://doi.org/10.1016/j.intermet.2015.03.013.

[46] I. Gurappa, Characterization of different materials for corrosion resistance under simulated body fluid conditions, Mater. Char. 49 (2002) 73–79, https://doi.org/10.1016/S1044-5803(02)00320-0.

[47] N. Rinčić, I. Baučić, S. Miko, M. Papić, E. Prohić, Corrosion behaviour of the Co-Cr-Mo dental alloy in solutions of different composition and different pH values, Coll. Antropol. 27 (2003) 99–106.

[48] C. Valero Vidal, A. Igual Muñoz, Effect of physico-chemical properties of simulated body fluids on the electrochemical behaviour of CoCrMo alloy, Electrochim. Acta 56 (2011) 8239–8248, https://doi.org/10.1016/j.electacta.2011.06.068.

[49] I. Mutlu, E. Oktay, Characterization of 17-4 PH stainless steel foam for biomedical applications in simulated body fluid and artificial saliva environments, Mater. Sci. Eng. C 33 (2013) 1125–1131, https://doi.org/10.1016/j.msec.2012.12.004.

[50] I.D. Dimić, I.L. Cvijović-Alagić, I.T. Kostić, A.A. Perić-Grujić, M.P. Rakin, S.S. Putić, B.M. Bugarski, OtpuŠtanje metalnih jona iz biokompatibilne legure kobalta, Chem. Ind. Chem. Eng. Q. 20 (2014) 571–577, https://doi.org/10.2298/CICEQ130813039D.

[51] M. Hurlbutt, B. Novy, D. Young, Dental caries: a pH-mediated disease, J Calif Dent Hyg Assoc 25 (2010) 9–15.

[52] G. Popescu, B. Ghiban, C.A. Popescu, L. Rosu, R. Truscă, I. Carcea, V. Soare, D. Dumitrescu, I. Constantin, M.T. Olaru, B.A. Carlan, New TiZrNbTaFe high entropy alloy used for medical applications, IOP Conf. Ser. Mater. Sci. Eng. 400 (2018), https://doi.org/10.1088/1757-899X/400/2/022049, 022049.

[53] J. Li, X. Yang, R. Zhu, Y. Zhang, Corrosion and serration behaviors of TiZr0.5NbCr0.5VxMoy high entropy alloys in aqueous environments, Metals 4 (2014) 597–608, https://doi.org/10.3390/met4040597.

[54] B. Ghiban, G. Popescu, C. Lazar, L. Rosu, I. Constantin, M. Olaru, B. Carlan, Corrosion behaviour in human stimulation media of a high entropy titan-based alloy, IOP Conf. Ser. Mater. Sci. Eng. 374 (2018), https://doi.org/10.1088/1757-899X/374/1/012004, 012004.

[55] A. Motallebzadeh, N.S. Peighambardoust, S. Sheikh, H. Murakami, S. Guo, D. Canadinc, Microstructural, mechanical and electrochemical characterization of TiZrTaHfNb and Ti1.5ZrTa0.5Hf0.5Nb0.5 refractory high-entropy alloys for biomedical applications, Intermetallics 113 (2019) 106572, https://doi.org/10.1016/j.intermet.2019.106572.
[56] Y.-L. Zhou, M. Niinomi, T. Akahori, Changes in mechanical properties of Ti alloys in relation to alloying additions of Ta and Hf, Mater. Sci. Eng. 483–484 (2008) 153–156, https://doi.org/10.1016/j.msea.2006.09.173.
[57] P.L. Ferrandini, F.F. Cardoso, S.A. Souza, C.R. Afonso, R. Caram, Aging response of the Ti–35Nb–7Zr–5Ta and Ti–35Nb–7Ta alloys, J. Alloys Compd. 433 (2007) 207–210, https://doi.org/10.1016/j.jallcom.2006.06.094.
[58] N. Tüten, D. Canadinc, A. Motallebzadeh, B. Bal, Microstructure and tribological properties of TiTaHfNbZr high entropy alloy coatings deposited on Ti 6Al 4V substrates, Intermetallics 105 (2019) 99–106, https://doi.org/10.1016/j.intermet.2018.11.015.
[59] A. Motallebzadeh, M.B. Yagci, E. Bedir, C.B. Aksoy, D. Canadinc, Mechanical properties of TiTaHfNbZr high-entropy alloy coatings deposited on NiTi shape memory alloy substrates, Metall. Mater. Trans. 49 (2018), https://doi.org/10.1007/s11661-018-4605-4, 1992–1997.
[60] T. Kokubo, H. Takadama, How useful is SBF in predicting in vivo bone bioactivity? Biomaterials 27 (2006) 2907–2915, https://doi.org/10.1016/j.biomaterials.2006.01.017.
[61] I. ASTM, ASTM G31-72: Standard Practice for Laboratory Immersion Corrosion Testing of Metals, Annu. B. ASTM Stand., 2004.
[62] S.-P. Wang, J. Xu, (TiZrNbTa)-Mo high-entropy alloys: dependence of microstructure and mechanical properties on Mo concentration and modeling of solid solution strengthening, Intermetallics 95 (2018) 59–72, https://doi.org/10.1016/j.intermet.2018.01.017.
[63] J.-P. Couzinié, G. Dirras, Body-centered cubic high-entropy alloys: from processing to underlying deformation mechanisms, Mater. Char. 147 (2019) 533–544, https://doi.org/10.1016/j.matchar.2018.07.015.
[64] F. Lukáč, M. Dudr, J. Čížek, P. Harcuba, T. Vlasák, M. Janeček, J. Kuriplach, J. Moon, H.S. Kim, J. Zýka, J. Málek, Defects in high entropy alloy HfNbTaTiZr prepared by high pressure torsion, Acta Phys. Pol., A 134 (2018) 891–894, https://doi.org/10.12693/APhysPolA.134.891.
[65] Y. Shi, B. Yang, P. Liaw, Corrosion-resistant high-entropy alloys, Rev. Metal. (Madr.) 7 (2017) 43, https://doi.org/10.3390/met7020043.
[66] Y.L. Chou, Y.C. Wang, J.W. Yeh, H.C. Shih, Pitting corrosion of the high-entropy alloy Co1.5CrFeNi1.5Ti0.5Mo0.1 in chloride-containing sulphate solutions, Corrosion Sci. 52 (2010) 3481–3491, https://doi.org/10.1016/j.corsci.2010.06.025.
[67] P.C. Pistorius, G.T. Burstein, Growth of corrosion pits on stainless steel in chloride solution containing dilute sulphate, Inf. Manag. 23 (1992) 1885–1897.
[68] Y.Y. Chen, T. Duval, U.D. Hung, J.W. Yeh, H.C. Shih, Microstructure and electrochemical properties of high entropy alloys—a comparison with type-304 stainless steel, Corrosion Sci. 47 (2005) 2257–2279, https://doi.org/10.1016/j.corsci.2004.11.008.
[69] B. Deng, Y. Jiang, J. Liao, Y. Hao, C. Zhong, J. Li, Dependence of critical pitting temperature on the concentration of sulphate ion in chloride-containing solutions, Appl. Surf. Sci. 253 (2007) 7369–7375, https://doi.org/10.1016/j.apsusc.2007.03.034.
[70] A. Ayyagari, R. Salloom, S. Muskeri, S. Mukherjee, Low activation high entropy alloys for next generation nuclear applications, Materialia 4 (2018) 99–103, https://doi.org/10.1016/j.mtla.2018.09.014.
[71] K.-K. Tseng, C.-C. Juan, S. Tso, H.-C. Chen, C.-W. Tsai, J.-W. Yeh, Effects of Mo, Nb, Ta, Ti, and Zr on mechanical properties of equiatomic Hf-Mo-Nb-Ta-Ti-Zr alloys, Entropy 21 (2018) 15, https://doi.org/10.3390/e21010015.
[72] A. Ayyagari, V. Hasannaeimi, H. Arora, S. Mukherjee, Electrochemical and friction characteristics of metallic glass composites at the microstructural length-scales, Sci. Rep. 8 (2018) 906, https://doi.org/10.1038/s41598-018-19488-7.
[73] L. Lilensten, J.P. Couzinié, J. Bourgon, L. Perrière, G. Dirras, F. Prima, I. Guillot, Design and tensile properties of a bcc Ti-rich high-entropy alloy with transformation-induced plasticity, Mater. Res. Lett. 5 (2017) 110–116, https://doi.org/10.1080/21663831.2016.1221861.
[74] T. Niendorf, D. Canadinc, H.J. Maier, I. Karaman, G.G. Yapici, Microstructure–mechanical property relationships in ultrafine-grained NbZr, Acta Mater. 55 (2007) 6596–6605, https://doi.org/10.1016/j.actamat.2007.08.015.
[75] B. Uzer, O. Birer, D. Canadinc, Investigation of the dissolution–reformation cycle of the passive oxide layer on NiTi orthodontic archwires, Shape Mem. Superelasticity. 3 (2017) 264–273, https://doi.org/10.1007/s40830-017-0114-3.
[76] S.M. Toker, D. Canadinc, Evaluation of the biocompatibility of NiTi dental wires: a comparison of laboratory experiments and clinical conditions, Mater. Sci. Eng. C 40 (2014) 142–147, https://doi.org/10.1016/j.msec.2014.03.060.
[77] C.L. Qin, W. Zhang, Q.S. Zhang, K. Asami, A. Inoue, Chemical characteristics of the passive surface films formed on newly developed Cu–Zr–Ag–Al bulk metallic glasses, J. Mater. Res. 23 (2008) 2091–2098, https://doi.org/10.1557/JMR.2008.0284.
[78] M.V. Popa, E. Vasilescu, P. Drob, C. Vasilescu, S.I. Drob, D. Mareci, J.C.M. Rosca, Corrosion resistance improvement of titanium base alloys, Quim. Nova 33 (2010) 1892–1896, https://doi.org/10.1590/S0100-40422010000900014.
[79] J.F. Watts, J. Wolstenholme, Electron spectroscopy: some basic concepts, in: An Introd. To Surf. Anal. by XPS AES, John Wiley & Sons, Ltd, Chichester, UK, 2005, pp. 1–15, https://doi.org/10.1002/0470867930.ch1.
[80] J. Jayaraj, D. Nanda Gopala Krishna, C. Mallika, U. Kamachi Mudali, Electrochemical studies and XPS analysis of the surface of zirconium-702 in concentrated nitric acid with and without fluoride ions, Trans. Indian Inst. Met. 71 (2018) 521–531, https://doi.org/10.1007/s12666-017-1165-z.
[81] C. Morant, J.M. Sanz, L. Galán, L. Soriano, F. Rueda, An XPS study of the interaction of oxygen with zirconium, Surf. Sci. 218 (1989) 331–345, https://doi.org/10.1016/0039-6028(89)90156-8.
[82] H.J.M. Bosman, A.P. Pijpers, A.W.M.A. Jaspers, An X-ray photoelectron spectroscopy study of the acidity of SiO2–ZrO2Mixed oxides, J. Catal. 161 (1996) 551–559, https://doi.org/10.1006/jcat.1996.0217.
[83] D.A. Stephenson, N.J. Binkowski, X-ray photoelectron spectroscopy of silica in theory and experiment, J. Non-Cryst. Solids 22 (1976) 399–421, https://doi.org/10.1016/0022-3093(76)90069-7.
[84] M.S. Amrutha, M. Tirumala Rao, S. Ramanathan, Mechanistic analysis of anodic dissolution of Zr in acidic fluoride media, J. Electrochem. Soc. 165 (2018) C162–C170, https://doi.org/10.1149/2.0851803jes.
[85] D. Majumdar, D. Chatterjee, X-ray photoelectron spectroscopic studies on yttria, zirconia, and yttria-stabilized zirconia, J. Appl. Phys. 70 (1991) 988–992, https://doi.org/10.1063/1.349611.
[86] Z. Li, Y. Liu, W. Kwapinski, J.J. Leahy, ZrO2-modified TiO2 nanorod composite: hydrothermal synthesis, characterization and application in esterification of organic acid, Mater. Chem. Phys. 145 (2014) 82–89, https://doi.org/10.1016/j.matchemphys.2014.01.037.
[87] A. Juma, I. Oja Acik, A.T. Oluwabi, A. Mere, V. Mikli, M. Danilson, M. Krunks, Zirconium doped TiO2 thin films deposited by chemical spray pyrolysis, Appl. Surf. Sci. 387 (2016) 539–545, https://doi.org/10.1016/j.apsusc.2016.06.093.
[88] J.-H. Xing, Z.-B. Xia, J.-F. Hu, Y.-H. Zhang, L. Zhong, Growth and crystallization of titanium oxide films at different anodization modes, J. Electrochem. Soc. 160 (6) (2013) C239–C246, https://doi.org/10.1149/2.070306jes.
[89] W.Y. Guo, J. Sun, J.S. Wu, Electrochemical and XPS studies of corrosion behavior of Ti-23Nb-0.7Ta-2Zr-O alloy in Ringer's solution, Mater. Chem. Phys. 113 (2–3) (2009) 816–820, https://doi.org/10.1016/j.matchemphys.2008.08.043.
[90] M.F. López, A. Gutiérrez, J.A. Jiménez, Surface characterization of new non-toxic titanium alloys for use as biomaterials, Surf. Sci. (2001) 300–305, https://doi.org/10.1016/S0039-6028(00)01005-0.
[91] C.C. Mohan, P.R. Sreerekha, V.V. Divyarani, S. Nair, K. Chennazhi, D. Menon, Influence of titania nanotopography on human vascular cell functionality and its proliferation in vitro, J. Mater. Chem. 22 (4) (2012) 1326–1340, https://doi.org/10.1039/c1jm13726c.